ACS OMEGA

Cite This: ACS Omega 2019, 4, 9569−9582

Article

http://pubs.acs.org/journal/acsodf

Mechanism of Thermal Degradation-Induced Gel Formation in Polyamide 6/Ethylene Vinyl Alcohol Blend Nanocomposites Studied by Time-Resolved Rheology and Hyphenated Thermogravimetric Analyzer Fourier Transform Infrared Spectroscopy Mass Spectroscopy: Synergistic Role of Nanoparticles and Maleic-anhydride-Grafted Polypropylene

Reza Salehiyan,*[,†,§] Jayita Bandyopadhyay,*[,†,§] and Suprakas Sinha Ray*[,†,‡]

[†]DST-CSIR National Centre for Nanostructured Materials, Council for Scientific and Industrial Research, Pretoria 0001, South Africa

[‡]Department of Applied Chemistry, University of Johannesburg, Doornfontein, 2028 Johannesburg, South Africa

Supporting Information

ABSTRACT: In this study, polyamide 6 (PA) is blended with ethylene vinyl alcohol (EVOH) to yield packaging materials with a balance of mechanical and gas barrier properties. However, the formation of gel-like structures in both polymers because of thermal degradation at high temperatures leads to a processing challenge, particularly during thin-gauge film extrusion. To address this challenge, nanoclays are introduced either directly or via a masterbatch of maleic-anhydride-grafted polypropylene to the PA/EVOH blend and time-resolved rheometry is used to study the effect of different modes of nanoclay incorporation on the kinetics of thermo-oxidative degradation of PA/EVOH blend and its nanocomposites. Time-resolved rheometry measurements allow the acquisition of accurate frequency-dependent linear viscoelastic behavior and offer insights into the rate of degradation or gel formation kinetics and cross-link density. The thermal degradation was studied by thermogravimetric analysis coupled with Fourier transform infrared spectroscopy and mass spectroscopy, allowing the prediction of the possible reactions that take place during the rheological property measurements. The results show that when nanoclays are incorporated directly, the oxidative reactions occur faster. In contrast, in the masterbatch method, oxidative degradation is hindered. The difference in the behaviors is shown to lie in the different nanoclay distributions in the blends; in the blends prepared by the masterbatch method, the nanoclays are dispersed at the interface. In conclusion, the masterbatch-containing blend nanocomposite would benefit processing and product development.

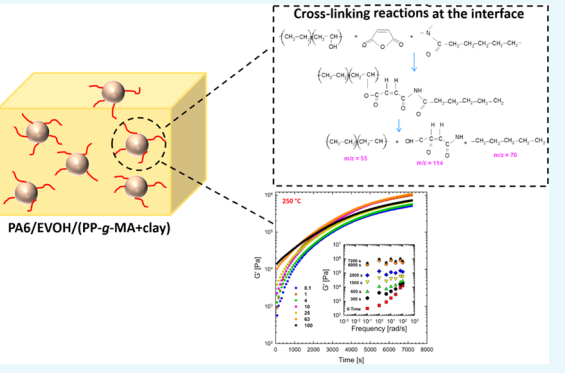

1. INTRODUCTION

Ethylene vinyl alcohol (EVOH) copolymer is a semicrystalline material with outstanding barrier properties against different gases and hydrocarbons, rendering it attractive for applications in food packaging.[1−5] However, the blending of two or more polymers is a popular and economical strategy for the development of new materials with adjustable properties depending on the polymer morphology. Thus, blends of EVOH with polyamide 6 (abbreviated as PA throughout the manuscript) could be an alternative material that preserves the permeability while improving the mechanical properties of the blends. On the other hand, it has been reported that the final performance of PA/EVOH blends is highly dependent on the ratio of the blend.[1−3] Yeh et al.[5] revealed that the minimum EVOH concentration required to preserve the crystal structure of EVOH is 20 wt % in a PA/EVOH blend. Because the crystalline regions are responsible for the permeation of molecules above this critical concentration (20 wt %), the oxygen permeation significantly increased. In another study, Incarnato et al.[3] revealed that the specific interactions in the amorphous regions between amide groups of PA and carboxyl groups of EVOH were strongest when the weight percentage ratio was 75/25 in a PA/EVOH blend. This composition led to a significant improvement in the rheological, morphological, and barrier properties of the blends. Also, recently, the use of inorganic nanoparticles in polymers is proven to be advantageous for enhancing the mechanical, thermal, and barrier properties.[6] However, the effectiveness of nanoparticle

Received: April 3, 2019
Accepted: May 20, 2019
Published: May 31, 2019

DOI: 10.1021/acsomega.9b00940
ACS Omega 2019, 4, 9569−9582

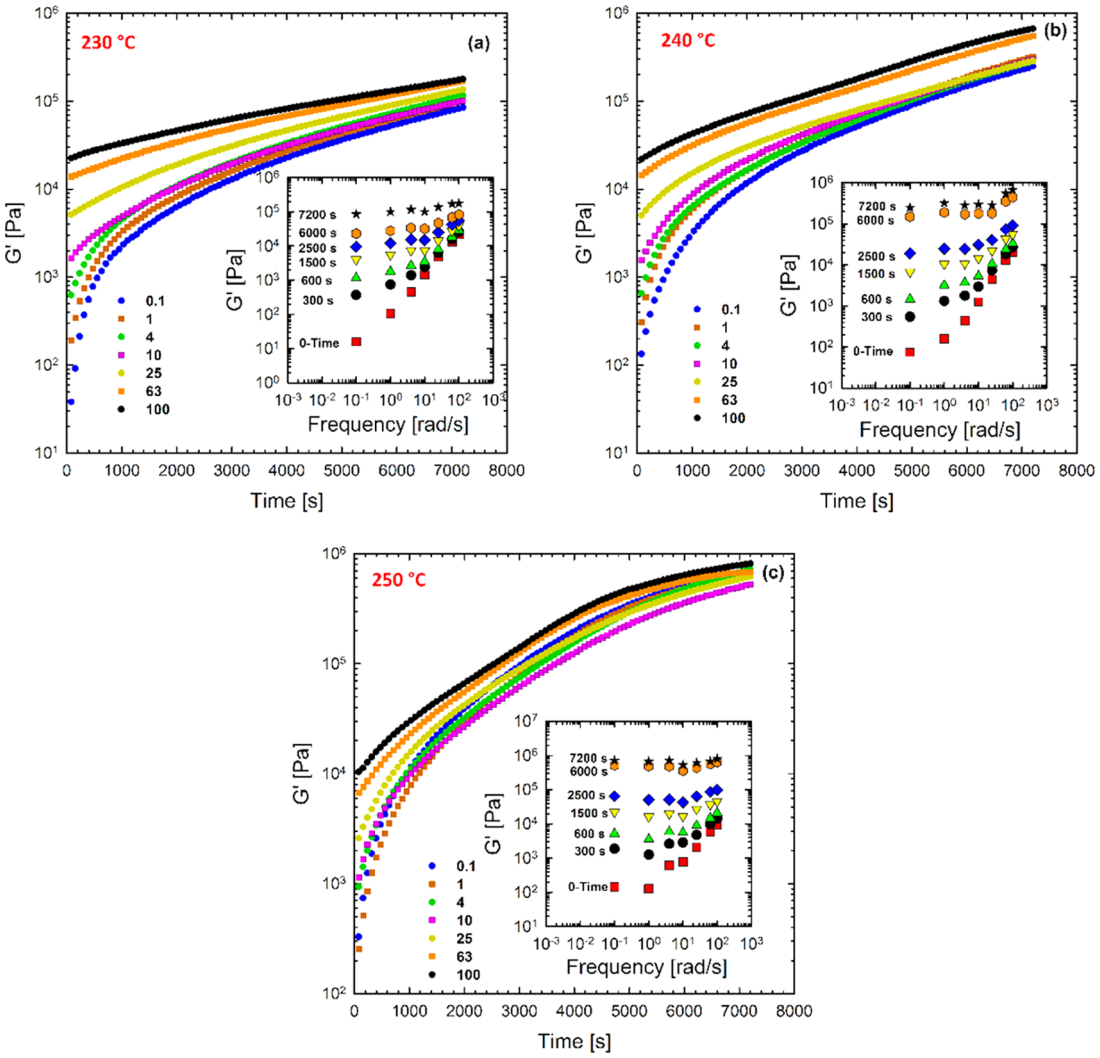

Figure 1. Time-resolved rheometry results for the elastic (storage) modulus ($G'(t)$) of the (80/20) PA/EVOH blend at different frequencies at a fixed-strain amplitude of 0.5% and temperatures of (a) 230, (b) 240, and (c) 250 °C under an air atmosphere. The inset plots show the isochronal elastic modulus ($G'(\omega_t)$) of the blends collected at different times (zero time, 300, 600, 1500, 2500, 6000, and 7200 s). PA, polyamide 6; EVOH, ethylene vinyl alcohol.

inclusion in improving the physical properties is known to be proportional to the distribution and dispersion of such nanoparticles within the polymer matrices. Furthermore, in the case of immiscible blends, it has been reported that optimized properties can be achieved when the nanoparticles are localized at the interface between the two phases.[7] That is, the localization of nanoparticles in immiscible blends can significantly affect the blend morphology and thus the final properties.

When nanoparticles are localized at the interface, they can act as a shield around the minor phase and suppress coalescence, thus stabilizing the morphology. The stabilized morphology, in turn, can improve the final properties as well.[7−9] In our previous study, different approaches to incorporate nanoclays into a 80/20 PA/EVOH blend were implemented.[10] It was found that when nanoclays were loaded via the masterbatch (maleic-anhydride-grafted polypropylene (PP-*g*-MA))/organically modified bentonite (BET) method into the blend, they were found at the interface and contributed to stabilizing the morphology by reducing the minor phase (EVOH) size. This is in contrast to the situation where the nanoclays were incorporated directly to the blend (PA/EVOH/BET). Furthermore, the rheological properties of the nanocomposites prepared via the masterbatch method were better than those of the directly processed nanocomposites. It is worth noting that the storage modulus ($G'(t)$) of the neat polymers and blends showed an increasing trend as a function of time, where the blends showed even more significant increases over time (Figure 10 of ref 10). This could be an indication of the interfacial interactions between PA and EVOH at high temperatures. It has been reported that PAs can decompose to alkoxy radicals in an oxidative atmosphere and further cross-linking interactions between such radicals and other reactive groups, e.g., amines and aldehydes, could lead to an increase in the modulus over time.[11,12] On the other hand, it has been revealed that EVOH can undergo oxidative degradation, transforming vinyl alcohol hydroxyl groups into carbonyl groups.[10,13] Such degradation, which affects the viscosity over time, could interfere with the rheological response of the material because the degradation time exceeds the relaxation time of the polymers. Frequency sweep tests are the most common and convenient methods to

DOI: 10.1021/acsomega.9b00940
ACS Omega 2019, 4, 9569−9582

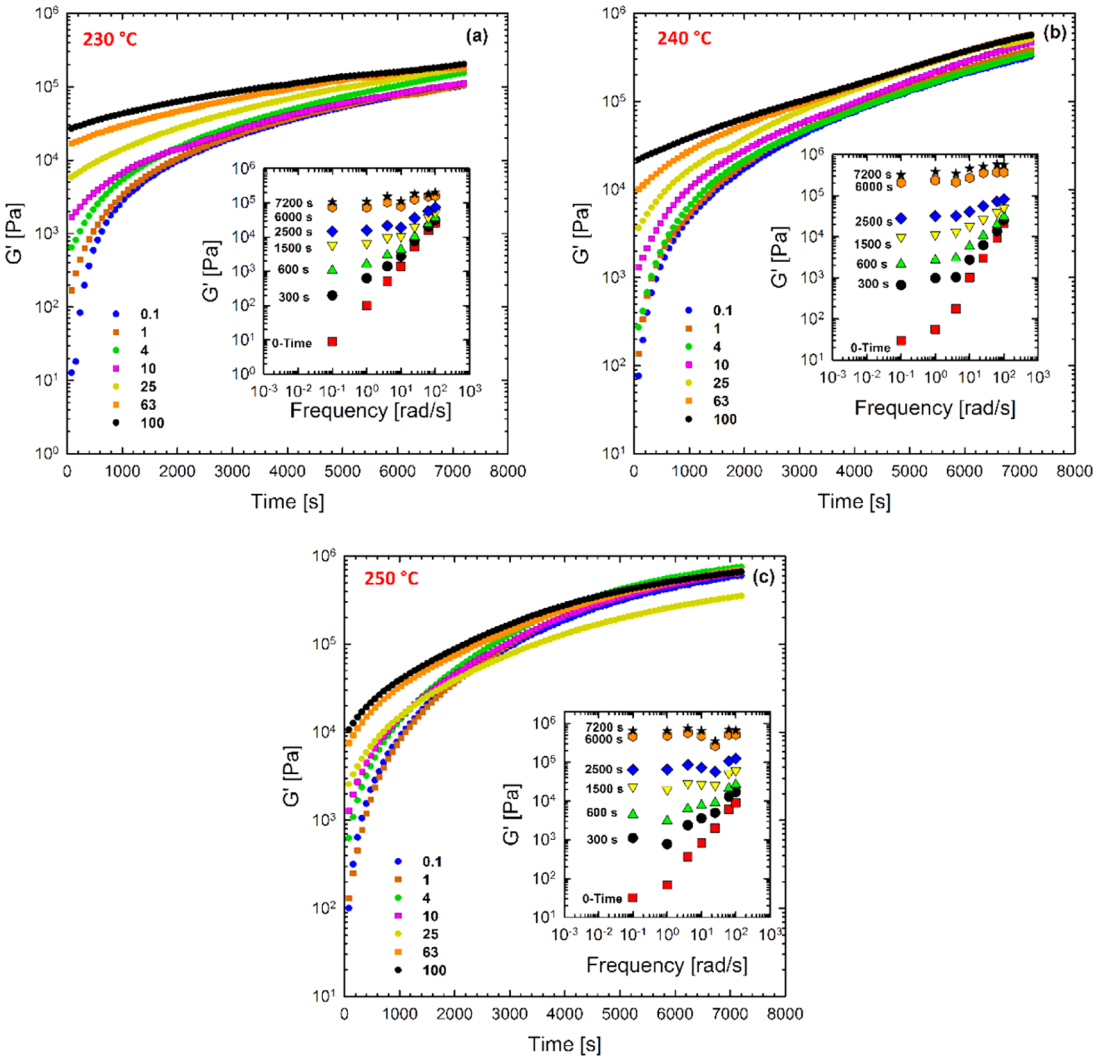

Figure 2. Time-resolved rheometry results for the elastic (storage) modulus ($G'(t)$) of the PA/EVOH/BET nanocomposite at different frequencies at a fixed-strain amplitude of 0.5% and temperatures of (a) 230, (b) 240, and (c) 250 °C under an air atmosphere. PA, polyamide 6; EVOH, ethylene vinyl alcohol; BET, organically modified montmorillonite.

study the linear rheological properties of materials. Moreover, more information can be obtained from low-frequency regions because it is associated with the longer relaxation time of polymers (larger portions of the materials). For instance, if the polymer is entangled, a longer time is required for relaxation; thus, a rubbery (plateau) region will appear at low frequencies (Chapter 6 of ref 14). Although the small imposed amplitude in the tests ensures that the structure of the materials will not be destroyed, in the case of transient polymers, degradation occurs faster than the relaxation, resulting in changes to the molecular structure of the materials.[15−17] Thus, the linear rheological results from frequency sweep tests may not be completely accurate because the molecular structure of the polymers changes as a result of degradation. Previous studies have revealed that time-resolved rheometry can be used to isolate the effects of degradation in the measurement of the rheological properties of such transient polymers.[15−18] In a time-resolved rheometry measurement, the frequency-dependent rheological properties of materials are obtained at various single fixed frequencies over a reasonable time; then, the zero-time properties are extrapolated to offset the effects of time and corresponding degradation.[15−19] In addition, it has been shown that the collection of isochronal storage moduli of PA/linear low-density polyethylene (PA/LLDPE) at different times can be used as an indication of the degree of cross-linking over time.[15]

Therefore, considering the effects of nanoclay localization on the structural properties of the blends and the fact that the blends are oxidatively degradable (as in the case of polymer gelation), the aims of the current study can be summarized as follows. The first objective of this study is to acquire an accurate frequency-dependent linear viscoelastic behavior of the (80/20) PA/EVOH blend, PA/EVOH/BET, PA/EVOH/MB nanocomposites, and PA/EVOH/PP-*g*-MA blend by excluding the degradation effects using time-resolved rheometry. The second objective is to examine the effect of nanoclay incorporation and localization on the rate and degree of degradation (cross-linking reactions). The third objective is to carry out objectives number 1 and 2 at different temperatures (230, 240, and 250 °C) to assess the effect of the atmospheric temperature on the viscoelastic and cross-linking behavior of the blends. The fourth and final objective of this study is to predict the probable cross-linking and degradation reaction mechanisms that occur during the rheological property

DOI: 10.1021/acsomega.9b00940
ACS Omega 2019, 4, 9569−9582

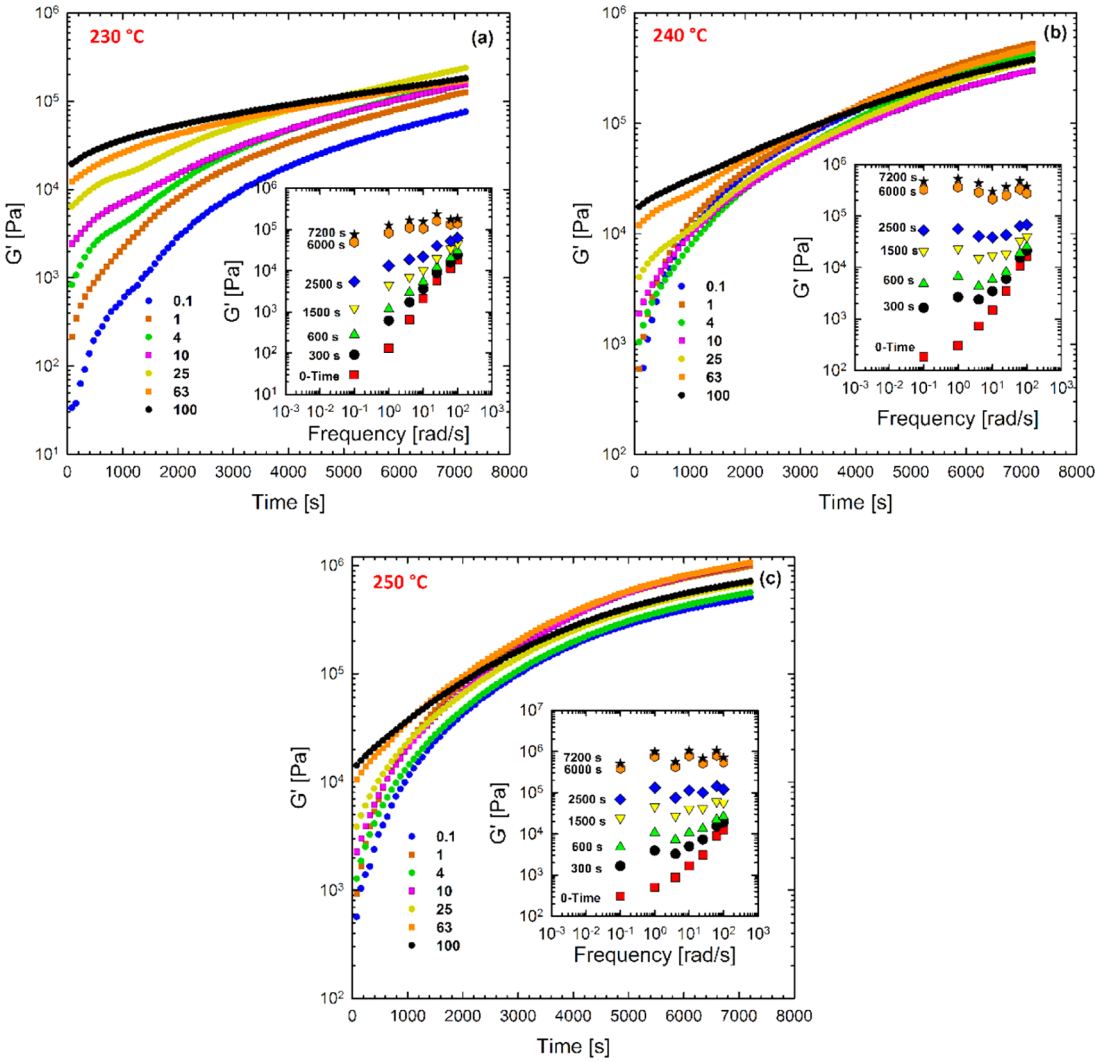

Figure 3. Time-resolved rheometry results for the elastic (storage) modulus ($G'(t)$) of the PA/EVOH/MB nanocomposite at different frequencies at a fixed-strain amplitude of 0.5% and temperatures of (a) 230, (b) 240, and (c) 250 °C under an air atmosphere. PA, polyamide 6; EVOH, ethylene vinyl alcohol; MB, masterbatch.

evaluation using online thermal degradation by thermogravimetric analysis coupled with Fourier transform infrared spectroscopy and mass spectroscopy (hyphenated TGA–FTIR–MS). This technique enables reaction monitoring in real time, and thus the predicted reactions can simulate the actual processing environment.

2. RESULTS AND DISCUSSION

2.1. Time Sweep Tests. To investigate the thermal stability, time-resolved rheometry measurements were performed on PA/EVOH (Figure 1), PA/EVOH/BET (Figure 2), PA/EVOH/MB (Figure 3), and PA/EVOH/PP-*g*-MA (Figure 4) at 230, 240, and 250 °C and different single-frequency scans. Because the elastic (storage) modulus (G') is more informative and sensitive to microstructural changes, G' as a function of time was plotted, as shown in Figures 1–4.[18]

From Figures 1 to 4, it can be seen that $G'(t)$ increases as a function of time, increasing rapidly initially and at lower frequencies and moderately increasing at later times and higher frequencies. It must be noted that the rates are also different at different temperatures, indicating the effect of temperature on the elastic moduli of the blends. Previous studies have correlated this behavior (increase in modulus over time) with the microstructural changes resulting from thermally induced reactions, such as cross-linking and branching.[15−17] In this particular case, such reactions can occur between alkoxy radicals and the amine groups with other carbonyl groups from EVOH because of the thermo-oxidative degradation of species that results in an increase in the viscosity and thus the modulus of the blend. This suggests possible interfacial (intermolecular) reactions between PA and EVOH in addition to the intramolecular reactions inside PA and EVOH. It is worth mentioning that in thermo-oxidative degradation, a balance between chain scission and cross-linking reaction determines the extent and rate of the increase of the modulus.[15] Thus, now that the thermo-oxidative nature of the blends has been revealed, the isochronal elastic modulus, $G'(\omega, t = 0, 300, 600, 1500, 2500, 6000,$ and 7200 s), at different frequencies can be collected at arbitrary times to plot the modulus as a function of frequency, as in the case of the frequency sweep tests. It has been previously discovered that conducting conventional frequency sweep tests on such degrading materials does not yield accurate results because the degradation time is faster than the relaxation time of the polymers at longer times (lower

DOI: 10.1021/acsomega.9b00940
ACS Omega 2019, 4, 9569−9582

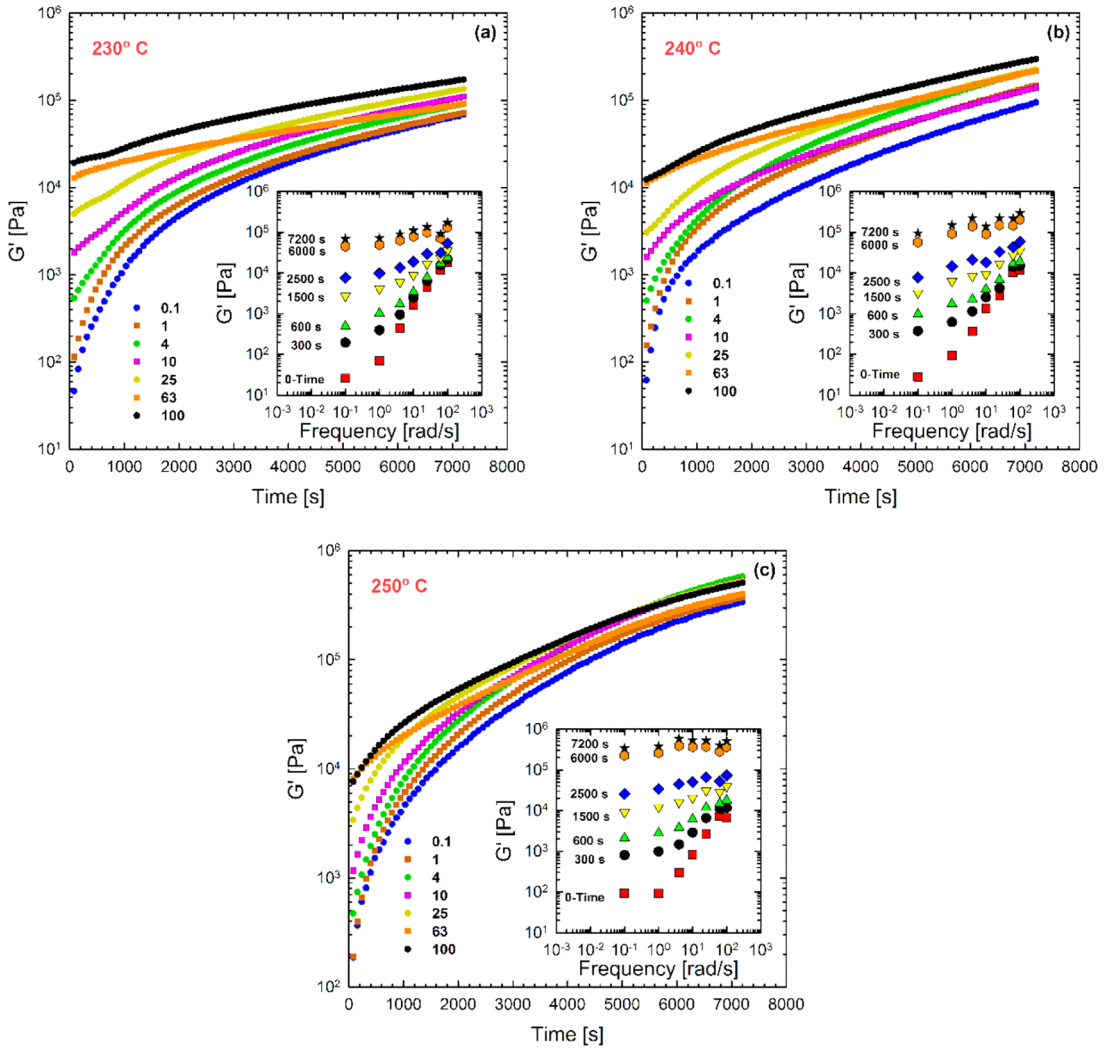

Figure 4. Time-resolved rheometry results for the elastic (storage) modulus ($G'(t)$) of the PA/EVOH/PP-*g*-MA blend at different frequencies at a fixed-strain amplitude of 0.5% and temperatures of (a) 230, (b) 240, and (c) 250 °C under an air atmosphere. PA, polyamide 6; EVOH, ethylene vinyl alcohol; PP-*g*-MA, maleic-anhydride-grafted polypropylene.

frequencies).[15] The results are shown in the insets of Figures 1−4. To eliminate the effect of the degradation, the moduli at zero time are extrapolated and plotted as a function of time. The other isochronal moduli at different times indicate the effect of time on the cross-linking reactions by showing an increase in the plateau modulus in the low-frequency regions of the inset plots (as discussed later). It is also difficult to distinguish the effect of temperature and the nanoclays on the degradation of the blends from Figures 1 to 4. One can use the gelation time (the time corresponding to the crossover point where $G'(t) = G''(t)$) to interpret the differences over time. To determine the G' and $G''(t)$ crossover points of the blends, a frequency of 0.1 rad/s was selected because a large portion of the molecules is subjected to shearing, which is associated with longer relaxation times. Therefore, the initial increase in the modulus is sharper at low frequencies. Figure 5 shows the gel time (crossover point) as a function of temperature for the blends and nanocomposites. The gel point was attained at shorter times when temperature increased for all samples. Figure 5 shows that, at 230 °C, the incorporation of the nanoclay retards the reaction between PA and EVOH. However, probing the issue from a different perspective illustrates that incorporation of nanoclays in PA/EVOH/BET

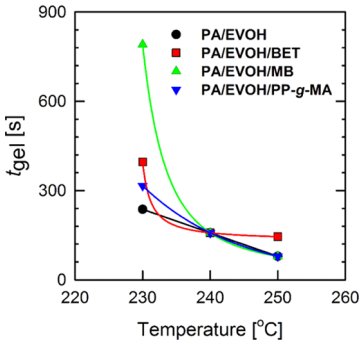

Figure 5. Gel point (crossover) evolution of PA/EVOH blend, PA/EVOH/BET nanocomposite, PA/EVOH/MB nanocomposite, and PA/EVOH/PP-*g*-MA blend as a function of the temperature acquired from time-resolved rheometry (time sweep tests) measurements at a frequency of 0.1 rad/s. PA, polyamide 6; EVOH, ethylene vinyl alcohol; BET, organically modified montmorillonite; MB, masterbatch; PP-*g*-MA, maleic-anhydride-grafted polypropylene.

nanocomposite led to faster reactions than PA/EVOH/MB nanocomposite but slower than PA/EVOH/PP-*g*-MA blend at 230 °C. This indicates the synergistic effect of PP-*g*-MA/BET

DOI: 10.1021/acsomega.9b00940
ACS Omega 2019, 4, 9569−9582

masterbatch on the degradation and the reaction rates. The reaction time (indicated by "t_{gel}" in Figure 5) follows the trend: PA/EVOH/MB > PA/EVOH/BET > PA/EVOH/PP-*g*-MA > PA/EVOH (at 230 °C). Therefore, the incorporation of the nanoclay effectively controls the thermal degradation and gel formation during melt processing at 230 °C. At 240 and 250 °C, t_{gel} remains similar in all samples. This can be interpreted from three perspectives: (i) increasing the temperature increases the reaction rate, (ii) the nanocomposites show higher elasticity compared to that of the neat blend, and (iii) nanoclay addition accelerates the rate of cross-linking reactions during degradation. To investigate these points, the isochronal collected moduli, $G'(t)$, at different frequencies were plotted to construct the frequency sweep results, as shown in Figures 6 and 7.

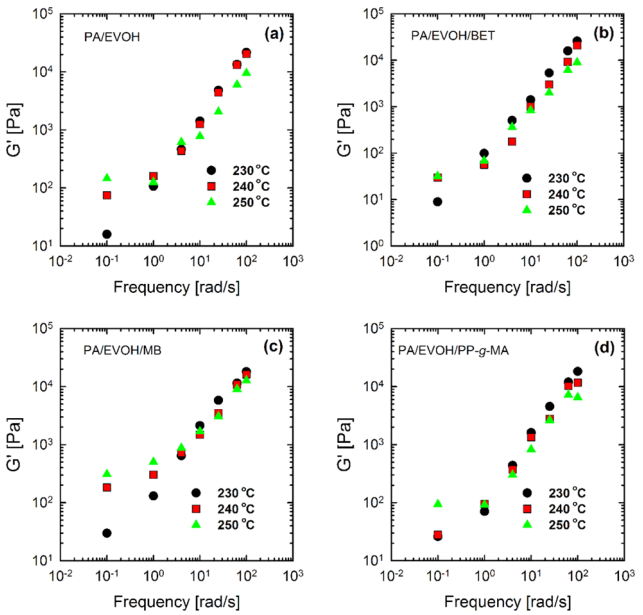

Figure 6. Isochronal zero-time elastic moduli $G'(\omega_{t=0})$ of (a) PA/EVOH, (b) PA/EVOH/BET, (c) PA/EVOH/MB, and (d) PA/EVOH/PP-*g*-MA samples collected at different times from time-resolved rheometry tests under an air atmosphere at 230, 240, and 250 °C. PA, polyamide 6; EVOH, ethylene vinyl alcohol; BET, organically modified montmorillonite; MB, masterbatch; PP-*g*-MA, maleic-anhydride-grafted polypropylene.

2.2. Effect of Measuring Temperature. As discussed previously, frequency sweep tests are straightforward and widely used to analyze the microstructure of materials. However, for transient polymers that undergo degradation reactions faster than the experimental time, the analysis of the frequency test results can be challenging. Therefore, the zero-time moduli were extrapolated from the time-resolved rheology results to fabricate the frequency sweep results via the point-to-point collection of moduli from all single scanned frequencies. Figure 6 shows the corresponding acquired zero-time elastic moduli ($G'(t = 0)$) of the blends at different temperatures used to observe the effect of temperature on the linear viscoelastic behavior of the blends. It is obvious from the plots that the elastic moduli $G'(\omega)$ in the low-frequency regions of all blends and nanocomposites is increased. It should be noted again that the low-frequency regions are richer in information because a larger portion of the molecule is being relaxed. Furthermore, the formation of a plateau modulus in the low-frequency region is an indication of entanglement or gel-like behavior, possibly arising from reactions between the radicals within the polymers and at the interface that leads to the creation of a copolymer at the interface (as discussed later). It is worth mentioning that in the case of PA/EVOH/BET nanocomposite, the increase in the low-frequency region moduli is less significant of all studied cases. A plateau in the modulus plot was not observed for the PA/EVOH/BET nanocomposite, suggesting that the direct addition of a nanoclay into the blend did not contribute to gel formation at the interface.

2.3. Effect of Nanoclay Localization on the Rate and Degree of Reactions. Microscopy results from a previous study (Figure 7) revealed that nanoclays are located at the interface of PA and EVOH in the case of PA/EVOH/MB nanocomposite.[10] Thus, the PP-*g*-MA (present in the masterbatch), which has a tendency to segregate at the interface of the blend and emulsify the morphology, would localize itself and the embedded nanoclays at the interface. Therefore, on the one hand, the nanoclays and PP-*g*-MA at the interface form a core−shell structure around the EVOH droplets where interfacial tension is reduced and coalescence is hindered. As a result, the encapsulated EVOH droplets can relax at longer times, causing the formation of a shoulder (plateau modulus) at low frequencies. On the other hand, nanoclays at the interface of the PP-*g*-MA shell could contribute to the reactions occurring at the interface between radicals of PA and EVOH, thus inducing the copolymer formation at the interface.

Therefore, it can be said that the gel-like behavior (plateau modulus at low frequency) of the PA/EVOH/MB and its larger values, G'_{ω} (PA/EVOH/MB) > G'_{ω} (PA/EVOH/PP-*g*-MA) > G'_{ω} (PA/EVOH/BET), is due to the emulsifying effect of the PP-*g*-MA/BET, which hinders the coalescence of the droplets and stabilizes the morphology. This again signifies the synergistic effect of PP-*g*-MA and BET nanoclays in the case of the PA/EVOH/MB nanocomposite. Figure 8 shows the zero-time elastic moduli $G'(t = 0)$ of the blends at fixed temperatures.

Interestingly, despite the size reduction observed in the morphology of PA/EVOH/BET, the zero-time elastic moduli $G'(\omega_{t=0})$ of the PA/EVOH/BET nanocomposites are the lowest at low to medium frequencies.[10] At this point, we must consider that the scanning electron microscopy (SEM, Figure 7) images were taken from cryo-fractured samples where exposure to high temperatures, as in the case of rheological measurement, was absent. Possibly, at the beginning of exposure at zero time, the radicals can freely react at the interface. In contrast, in the case of the PA/EVOH/BET nanoclays, which are dispersed within the polymer matrix, a slightly longer time is required for the reaction to occur. In other words, in PA/EVOH/BET, at zero time, the reactions in PA/EVOH have a dominant effect in defining the form of the elastic modulus compared with the effect of nanoclay inclusion.

Moreover, this suggests that the reactions are also shear-sensitive. The existence of nanoclays can cause frictional forces between platelets and polymer chains, inducing reactions and enhancing the moduli as a function of time during shearing. To understand the effect of nanoclay addition and its localization on the rate and degree of cross-linking reactions further, the plateau modulus, G_N, from the inset plots of Figures 1−4 was analyzed and used as an indication of the degree of cross-linking (see Figure 9).

DOI: 10.1021/acsomega.9b00940
ACS Omega 2019, 4, 9569−9582

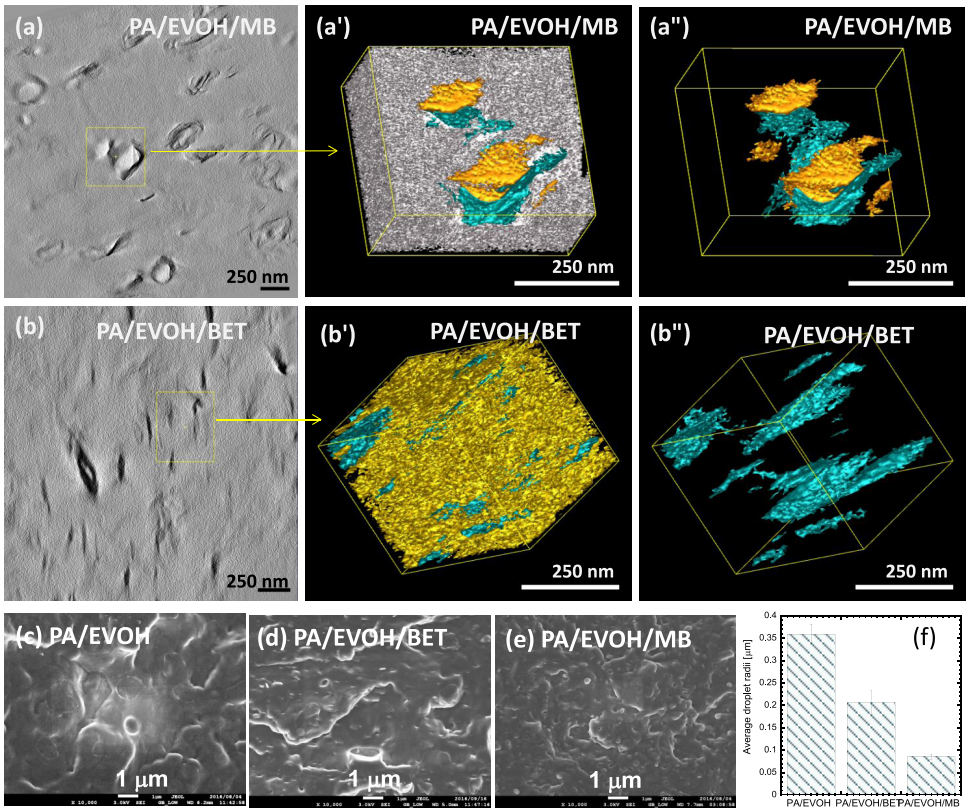

Figure 7. Three-dimensional (3D) tomogram from transmission electron microscopy images showing the nanoclay distributions in (a, a′, a″) PA/EVOH/MB and (b, b′, b″) PA/EVOH/BET nanocomposites. The silver, blue, golden, and yellow background colors represent the PA, nanoclays, EVOH and PA/EVOH blend, respectively. The cryogenically fractured scanning electron microscopy (SEM) surface images of (c) PA/EVOH, (d) PA/EVOH/BET, and (e) PA/EVOH/MB. (f) The number-averaged droplet radii (R_n) was estimated by analyzing 50−100 droplets from several SEM images captured for each sample.[10] Copyright 2017. It is reproduced with permission from Elsevier Ltd. PA, polyamide 6; EVOH, ethylene vinyl alcohol; BET, organically modified montmorillonite; MB, masterbatch.

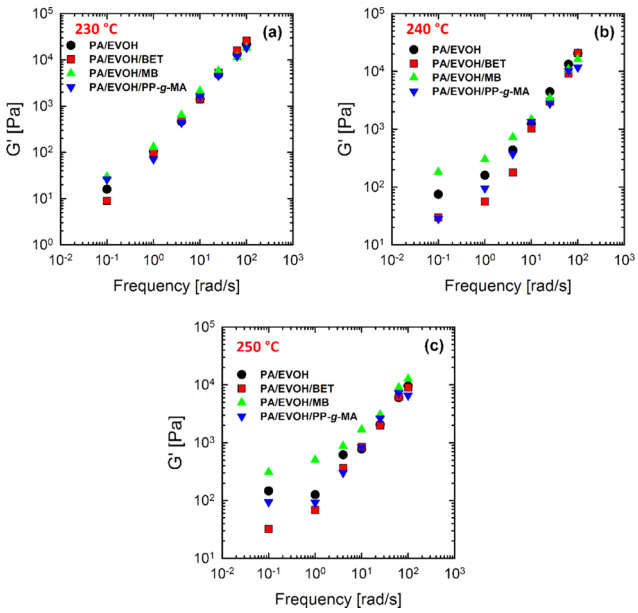

Figure 8. Isochronal zero-time elastic moduli $G'(\omega_{t=0})$ of the PA/EVOH blend, PA/EVOH/BET nanocomposite, PA/EVOH/MB nanocomposite, and PA/EVOH/PP-*g*-MA blend collected at different times from time-resolved rheometry tests under an air atmosphere at (a) 230, (b) 240, and (c) 250 °C. PA, polyamide 6; EVOH, ethylene vinyl alcohol; BET, organically modified montmorillonite; MB, masterbatch; PP-*g*-MA, maleic-anhydride-grafted polypropylene.

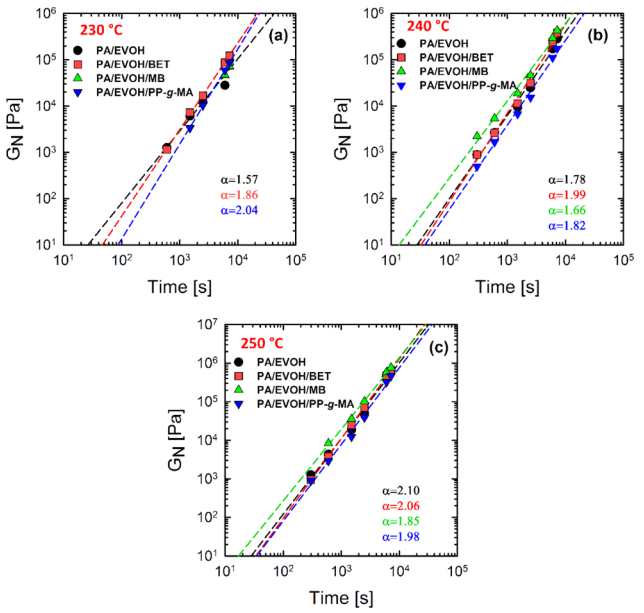

Figure 9. Plateau moduli (G_N) of the PA/EVOH blend, PA/EVOH/BET nanocomposite, PA/EVOH/MB nanocomposite, and PA/EVOH/PP-*g*-MA blend as a function of time at (a) 230, (b) 240, and (c) 250 °C extracted from inset plots in Figures 1−4. PA, polyamide 6; EVOH, ethylene vinyl alcohol; BET, organically modified montmorillonite; MB, masterbatch; PP-*g*-MA, maleic-anhydride-grafted polypropylene.

DOI: 10.1021/acsomega.9b00940
ACS Omega 2019, 4, 9569−9582

The log−log plots of the plateau modulus (G_N) as a function of time (Figure 9) yielded a straight line for the blends with different slopes (α) at different temperatures and nanoclay localizations. Interestingly, the slopes are highest for PA/EVOH/BET at higher temperatures, indicating that the localization of the nanoclay within the PA/EVOH blend matrix accelerates the chain scission (see Section 2.4) reaction. In contrast, when nanoclays were introduced via a masterbatch method and localized at the interface (PA/EVOH/MB), the slopes are the lowest at all temperatures despite the higher moduli values. From the above findings, the two effects (the rate of reaction and degree of cross-linking) can be differentiated. It is consistent with the theory of diffusion-controlled reactions where the higher the viscosity, the lower the diffusion as well as the rate of reaction would be. To demonstrate the ultimate degree of cross-linking after 2 h (7200 s), the plateau modulus from the ultimate isochronal storage modulus, $G'(\omega_{t=7200})$, was used to calculate the cross-link density (XD) using the following equation.[20]

$$\mathrm{XD} = \frac{G_N}{6RT} \quad (1)$$

Here, G_N is the plateau storage modulus at 7200 s, R is the gas constant, and T is the absolute temperature. The calculated cross-link densities of the blends are plotted in Figure 10 as a function of temperature.

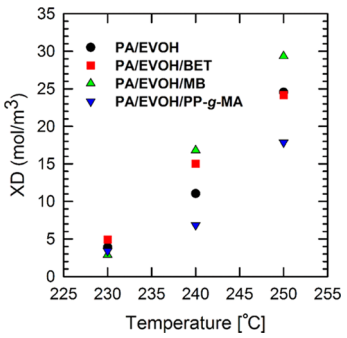

Figure 10. Calculated cross-link densities of PA/EVOH blend, PA/EVOH/BET nanocomposite, PA/EVOH/MB nanocomposite, and PA/EVOH/PP-*g*-MA blend from the plateau moduli (G_N) at 7200 s at different temperatures. PA, polyamide 6; EVOH, ethylene vinyl alcohol; BET, organically modified montmorillonite; MB, masterbatch; PP-*g*-MA, maleic-anhydride-grafted polypropylene.

Figures 9 and 10 reveal that the reactions are temperature sensitive and at higher temperatures, the cross-links became more significant. Moreover, despite the faster rate observed for PA/EVOH/BET, the PA/EVOH/MB nanocomposites showed higher cross-link densities. That is, in the case of nanocomposites prepared via the masterbatch method, the cross-linking reactions saturated the system at very early stages of the process. Thus, over time, fewer and fewer active sites were available for reaction as the viscosity increased and restricted the diffusion. Thus, the reaction rate was slower compared to that of the PA/EVOH/BET nanocomposites.

In addition, rheokinetic approaches were used to study the isothermal cross-linking reactions over the course of 2 h time sweep tests (see the Supporting Information (SI)).[21−23] The extent of reactions was measured using the rheological degree of conversion β as a function of time (Figure 1S, Supporting Information, SI). Further, the rate of conversions as a function of conversions $\left(\frac{d\beta}{dt} \text{ vs } \beta\right)$ can also be plotted (Figure 2S, SI). Then, the plots were fitted using eqs 2S and 4S (SI). It is interesting to see that the rate of conversions reached the plateau region at lower conversions in PA/EVOH/MB and PA/EVOH/BET at 250 °C (Figure 2Sb,c, SI). This indicates that in the systems where nanoclays are involved, the conversions occurred in a faster rate and reached the plateau region at earlier stages probably due to the induction role of nanoclays in the reactions.

Moreover, considering that PP-*g*-MA/BET at the interface contributed to the reactions at the interface and the fact that a stabilized interface has a significant effect on the moduli of the blends, the higher cross-linking density, as well as moduli, in the case of the PA/EVOH/MB nanocomposites can be explained. Possibly, the amine groups in the surfactant of the clays, as well as carbonyl groups of the anhydride can react with radicals from EVOH, meaning that more active groups contributed to the cross-linking reactions at the interface. On one hand, the MA group of the PP-*g*-MA could react with the amine end group of PA and form a copolymer.[24] On the other hand, the anhydride MA group on the polyolefins can react with the hydroxyl group of EVOH, leading to an increase in the viscosity of EVOH caused by gelation (as demonstrated in Section 2.4).[25] Further, the degradation of the nanoclay surfactant produces α-olefins that can also react with hydrogen atoms available in the system, accelerating the cross-linking reactions.[17] Other studies have also reported an increase in the cross-linking densities of nanocomposites because of reactions between organically modified nanoclays and polyacrylamide[26] and polyurethane.[27,28] The results reveal the critical role of nanoclay localization and the mode of inclusion on the rate and degree of the cross-linking reactions.

2.4. Degradation Reaction Mechanisms Studied by Hyphenated TGA−FTIR−MS. The coupling of TGA with FTIR and MS measurements allows the monitoring of the temperature and time-dependent degradation or cross-linking of PA/EVOH, PA/EVOH/BET, and PA/EVOH/MB observed during rheological property evaluation. The details of the experiments are described in the Supporting Information and shown in Figure 3S, SI. The FTIR spectra of the gas molecules emitted from TGA during isothermal (at 230 and 240 °C) and ramping temperature measurements are presented in Figures 11 and 12, respectively. The corresponding mass spectra at the beginning (ca. 5 min) and the end (ca. 118 min) of the isothermal periods are shown in Figures 4S−6S (SI), respectively. MS spectra selected at different times during the temperature ramp experiments are presented in Figures 7S and 8S (SI).

Figure 11a shows that at 230 °C, carbon dioxide (CO_2), secondary NH (H-bonding of PA), amide II (NH_2), and amide III (CN) bonds are present in PA/EVOH. The bands corresponding to these groups become more pronounced at 240 °C (Figure 11a′). This is in line with the time-resolved rheometry results because the rate of chain scission followed by the chain restructuring increases at 240 °C (the proposed reaction mechanism is shown in Schemes 1−3). Because the TGA experiments were conducted in a nitrogen atmosphere and the MS experiments were conducted in a helium atmosphere, the CO_2 may have been released from the degradation of EVOH and PA macromolecules. In the spectrum of PA/EVOH/BET, the CO_2 band is more pronounced and secondary NH, NH_2, and CN vibrations are

DOI: 10.1021/acsomega.9b00940
ACS Omega 2019, 4, 9569−9582

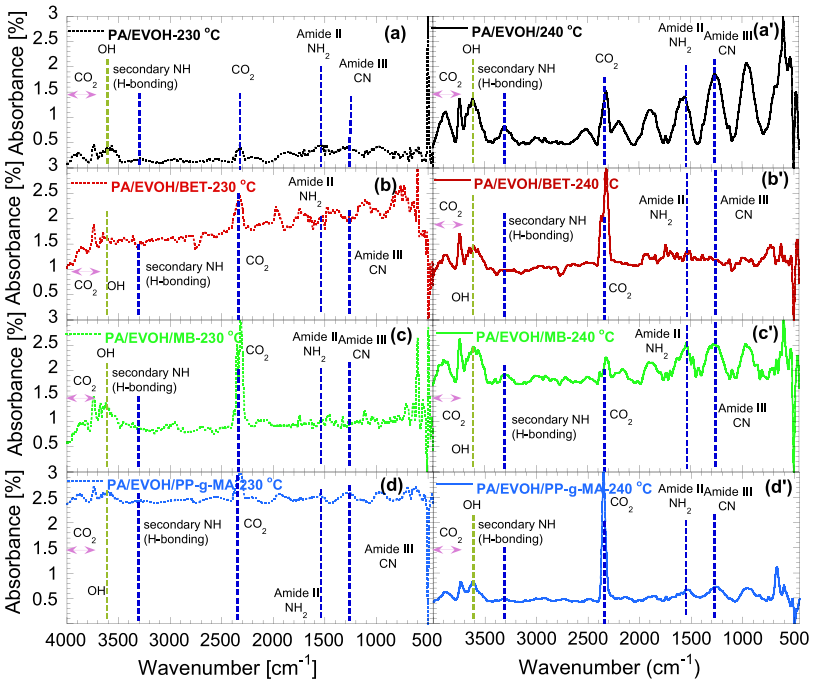

Figure 11. FTIR analysis of the gas evolved during thermal degradation (studied by hyphenated TGA−FTIR−MS) of PA/EVOH blend, PA/EVOH/BET nanocomposite, PA/EVOH/MB nanocomposite, and PA/EVOH/PP-*g*-MA blend at isothermal temperatures of (a−d) 230 and (a′−d′) 240 °C. PA, polyamide 6; EVOH, ethylene vinyl alcohol; BET, organically modified montmorillonite; MB, masterbatch.

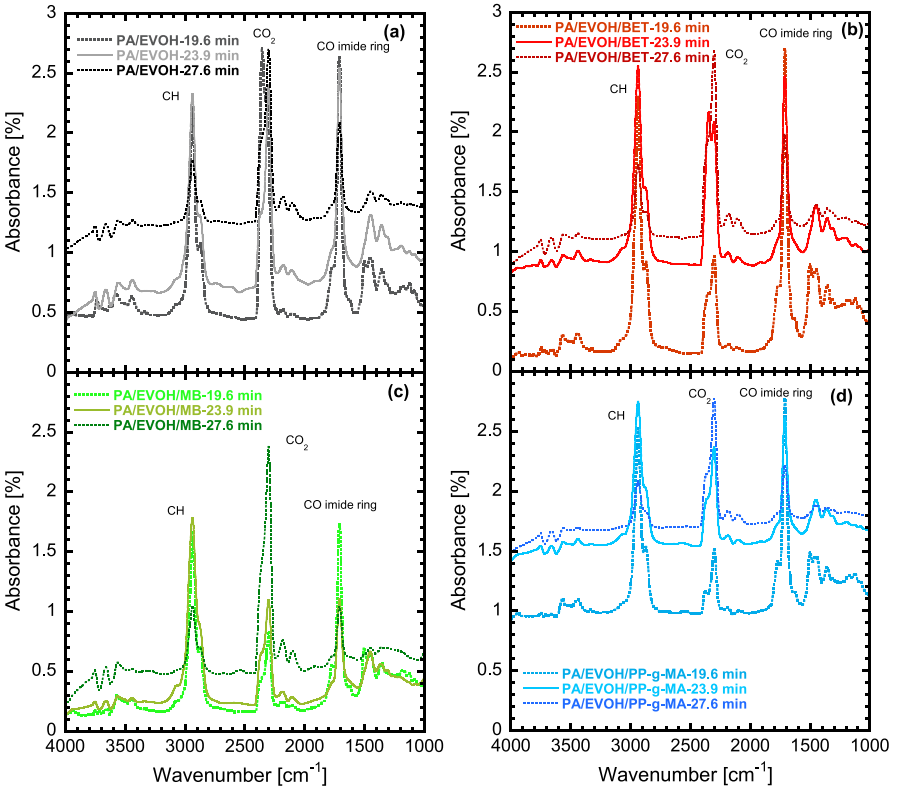

Figure 12. FTIR analysis of the gas evolved during thermal degradation (studied by hyphenated TGA−FTIR−MS) of (a) PA/EVOH blend, (b) PA/EVOH/BET nanocomposite, (c) PA/EVOH/MB nanocomposite, and (d) PA/EVOH/PP-*g*-MA blend. PA, polyamide 6; EVOH, ethylene vinyl alcohol; BET, organically modified montmorillonite; MB, masterbatch.

absent (Figure 11b). The distributed nanoclays in the PA/EVOH matrix most probably disrupt the inherent hydrogen bonding of PA and promote the chain scission and restructuring reactions. Consequently, the FTIR shows pronounced CO_2 absorption and the absence of secondary NH, NH_2, and CN vibrations. Such a reaction is probably responsible for the lowest G' observed during rheological property analysis of PA/EVOH/BET at all examined temper-

DOI: 10.1021/acsomega.9b00940
ACS Omega 2019, 4, 9569−9582

Scheme 1

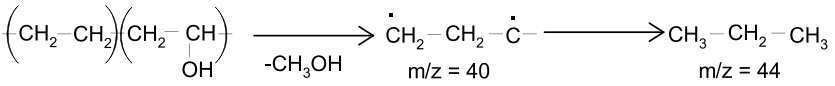

Scheme 2

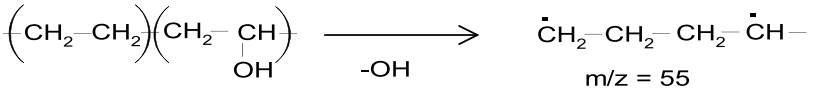

Scheme 3

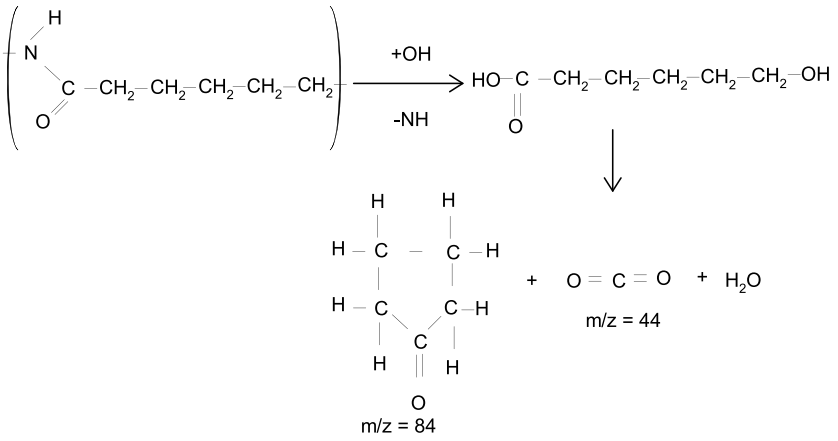

Scheme 4

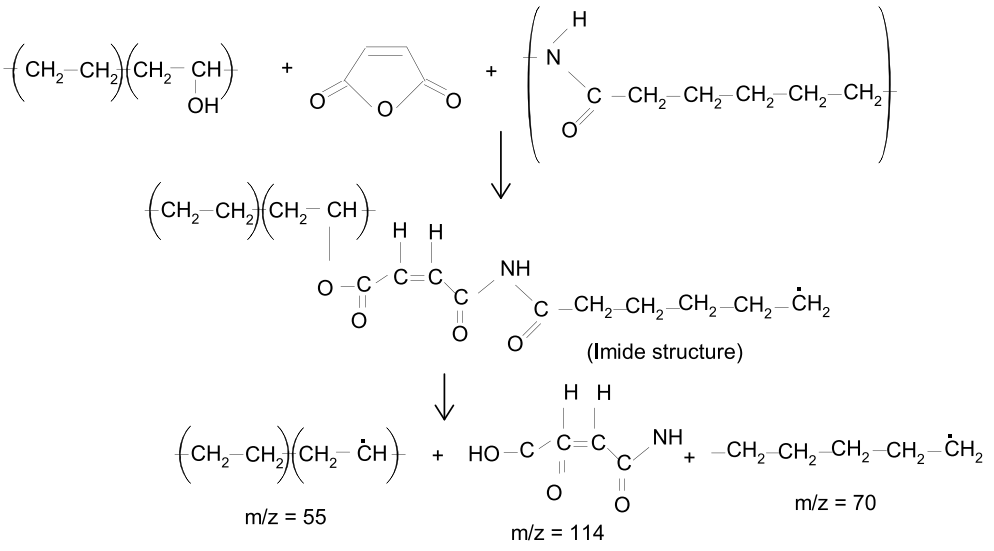

atures (see Figure 8). The increase in temperature enhances the reaction kinetics and the associated molecular vibrations (Figure 11b′). As revealed in Figure 11c,c′, the release of CO_2 from PA/EVOH/MB at 230 °C was more significant than that at 240 °C. Moreover, secondary NH, NH_2, and CN vibrations are still present at this temperature. This observation suggests that the EVOH core could undergo chain scission and that the cross-linking of EVOH, PP-*g*-MA (present in the MB), and PA begins at the interface. On the other hand, the spectrum of PA/EVOH/PP-*g*-MA is similar to that of PA/EVOH, although with stronger CO_2 absorption (Figure 11d,d′). As evidenced from the 3D tomograms (Figure 7), the BET nanoclays embedded in PP-*g*-MA are localized at the interface of PA and EVOH, thus retarding the overall rates of chain scission and the restructuring of PA and EVOH. However, at the interface, PP-*g*-MA bonds with both PA and EVOH phases, thus forming cross-linked structures. Bondon et al.[29] studied the interface morphology of PA and PP-*g*-MA as well as EVOH and PP-*g*-MA in a multilayered co-extruded film where PP-*g*-MA was used as a tie layer. The authors found that the interface of EVOH/PP-*g*-MA is much thicker than the interface of PA/PP-*g*-MA, indicating the formation of a complex copolymer architecture. As a result, PA/EVOH/MB exhibits a high cross-link density and hence high G' in the low-frequency region.

Although the reactions at isothermal temperatures result in some chain scission and recombination and gel formation,

DOI: 10.1021/acsomega.9b00940
ACS Omega 2019, 4, 9569−9582

Scheme 5

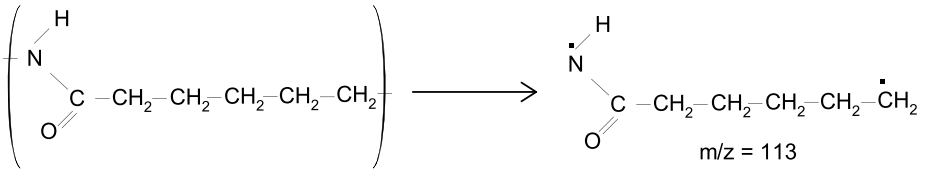

Scheme 6

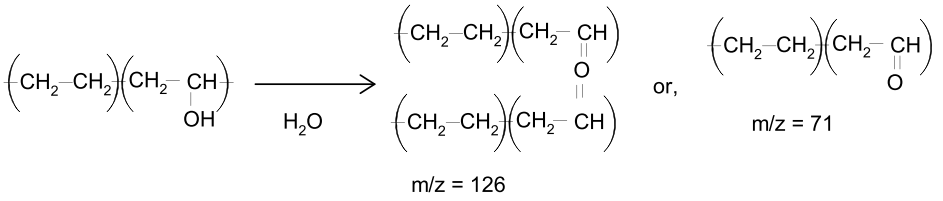

most degradation occurs in the range of 416−432 °C (ca. 19.6 min), followed by a significant step at 504−517 °C (ca. 23.9 min) (Figure 3Sc,d). Hence, the FTIR and MS spectra during the temperature ramp are reported at 19.6, 23.9, and 27.6 min (toward the end of the degradation). The FTIR spectra presented in the different parts of Figure 12 confirm the presence of CH, CO_2, and CO-imide rings in all samples, and a symmetrical imide C═O vibration appears at 1720 cm^{-1}.[30]

The reaction mechanisms are proposed on the basis of the mass fragments identified in Figures 4S−8S. According to Figures 4S and 5S, the pre-dominant mass-to-charge ratios (m/z) are 40 and 44. Additionally, a mass fragment with m/z = 44 appeared to a greater extent in PA/EVOH compared with the other samples. PA/EVOH/PP-*g*-MA showed the lowest emission of this mass fragment. Therefore, mass fragment 44 probably originates from the reaction of PA and EVOH. On the other hand, the mass fragments effused from the different samples during temperature ramping (in particular at 23.9 min) are at m/z = 40, 44, 55, 70, 84, and 113. The hydroxyl group of EVOH can react directly with the carboxyl end group of PA and forms slightly cross-linked extended chains.[31] Because the fragments at m/z = 40 and 44 are the dominant mass components, it is most likely that methanol is released from EVOH, as shown in reaction mechanism Scheme 1. The intermediate mass fragment has a mass of 40 and, after capturing hydrogen from propane, which has m/z = 44, a peak at m/z = 55 results from the breakdown of the C−O bond of EVOH (reaction Scheme 2). The free OH from EVOH reacts with PA and forms adipic acid, which eventually reduces to cyclopentane (m/z = 84), CO_2 (m/z = 44), and H_2O at around 285−295 °C (demonstrated in reaction Scheme 3).[32] In PA/EVOH/MB, at the interface region, PP-*g*-MA reacts with both polymers, as shown in reaction Scheme 4, and forms cross-linked structures. The formation of long chains in an intermediate step could be responsible for the initial high cross-link densities in PA/EVOH/MB, as shown in Figure 10. At high temperatures, this structure can eventually produce species with m/z = 55, 114, and 70 (demonstrated in reaction Scheme 4). Chain scission of PA itself results in species with m/z = 113 (demonstrated in reaction Scheme 5). It is apparent from Figures 6S to 8S (SI) that the release of the fragment at m/z = 113 is reduced significantly in the presence of the masterbatch. Therefore, the masterbatch can potentially retard the degradation of PA. Concerning gel formation in neat EVOH, the vinyl alcohol hydroxyl groups are transformed to carbonyl groups, thus creating a double bond (shown in reaction Scheme 6).[4] This may lead to the release of species at m/z = 71 and 126. The peak at m/z = 126 is absent in all MS spectra. However, in Figure 7S, the peak at m/z = 71 is only present in the spectra of PA/EVOH/MB and PA/EVOH/PP-*g*-MA. Therefore, the incorporation of the nanoclay via masterbatch can improve the thermal stability of PA/EVOH by preventing the degradation of both PA and EVOH. Moreover, from the above discussion, it is clear that the observed plateau behavior in the time-resolved rheometry may be due to the cross-linking reactions, as well as polymer chain restructuring, after a certain extent of chain scission.

Reaction Schemes 1−6. Probable reaction mechanisms associated with the reaction of PA and EVOH and interfacial cross-linking. m/z, mass-to-charge ratio.

3. CONCLUSIONS

The main objective of this work was to understand the effects of the incorporation of nanoclay particles and their localization on the rate and degree of degradation of a PA/EVOH blend using time-resolved rheometry and hyphenated TGA−FTIR−MS. Because all blends show a rapid increase in $G'(t)$ at shorter times and a moderate increase at longer times, the zero-time moduli ($G'(t = 0)$) were collected isochronally from all single-scan frequencies to manually construct the frequency sweep results. By doing so, the effects of thermal degradation were mitigated and more accurate frequency sweep results were obtained. It has also been revealed that increasing the measuring temperature increases the rate of intramolecular reactions, as well as those between radicals of both components: PA and EVOH. It is interesting to note that the direct addition of the nanoclay into the blend does not contribute to cross-link formation at the interface. The cross-link formation reaction takes place at the interfacial region of PA/EVOH/MB and thus this specimen exhibits a high cross-link density due to the synergistic effects of nanoclays and PP-*g*-MA. It was shown that the higher modulus of the PA/EVOH/MB was due to the interactions that both nanoclays and PP-*g*-MA caused at the interface concurrently. This was proved where moduli of each PA/EVOH/BET and PA/EVOH/PP-*g*-MA where lower than that of PA/EVOH/MB.

Reaction mechanisms have been proposed on the basis of the analysis of the released mass fragments obtained from hyphenated TGA−FTIR−MS measurements. The reaction schemes indicate that the observed plateau behavior in the

DOI: 10.1021/acsomega.9b00940
ACS Omega 2019, 4, 9569−9582

Scheme 7. Experimental Conditions of TGA−FTIR−GC−MS under (a) Isothermal Conditions at 230 and 240 °C and (b) Temperature Ramping from 50 to 900 °C at a Rate of 20 °C/min

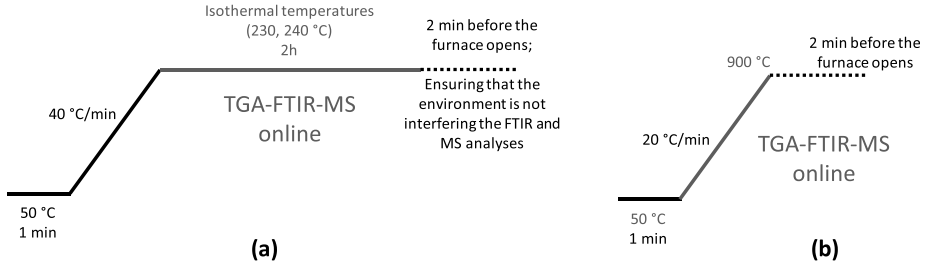

time-resolved rheometry measurements arises from the cross-linking reaction in PA/EVOH/MB. On the other hand, polymer chain restructuring after a certain extent of chain scission is mainly responsible for the plateau behavior observed in the PA/EVOH and PA/EVOH/BET blends. Therefore, if gel formation is defined as molecular restructuring caused by thermal degradation, the incorporation of the nanoclay masterbatch can reduce the rate of gel formation and increase the cross-link density at the interface. It was found that the reduced gel formation can thus decrease the die swelling of such nanocomposites. Further, on the basis of the melt flow index (MFI) value (≈8 g, 10 min^{-1}) of this particular blend nanocomposite (PA/EVOH/MB), we can suggest that it would be more suitable for rigid packaging (container) application (Figure 7 of ref 10). However, further studies on the barrier properties of this blend are required to confirm the link between nanoclay incorporation and oxygen permeability.

4. EXPERIMENTAL SECTION

4.1. Materials. The PA used in this study was a commercial product (UBE1015, UBE Industries, Japan). According to the supplier, the density of PA is 1.14 g/cm^3 and it melts between 215 and 225 °C. The measured melt flow index (MFI) (250 °C/2.16 kg) of PA is 4.56 g/10 min. The EVOH was commercial grade (Eval H171B, UBE Industries, Belgium) with 38 wt % ethylene content. The measured MFI of EVOH at 230 °C/2.16 kg is 3.41 g/10 min. The nanoclay, Betsopa OM (BET), is a South African natural bentonite modified with dimethyl dihydrogenated tallow quaternary ammonium surfactant. According to thermogravimetric analysis, BET contains approximately 36 wt % of surfactant and it was a commercial product obtained from CSIR, South Africa. The PP-*g*-MA/BET masterbatch (Polyzimo MB) is another in-house product with inorganic nanoclay content of around 30.8 wt %.

4.2. Sample Preparation. A twin-screw extruder (Process 11 co-rotating, L/D = 40, Thermo Scientific) was used to prepare the blends of PA and EVOH, as well as the nanocomposites. More detailed specifications on the preparation can be found in the previous work.[10] The blend and the nanocomposites with BET and masterbatch are denoted PA/EVOH, PA/EVOH/BET, and PA/EVOH/MB, respectively. A PA/EVOH/PP-*g*-MA sample was also prepared and analyzed to probe the reaction mechanism for the sake of comparison with the systems incorporated with nanoclays. Because of the hygroscopic nature of the polymers, the injection molded specimens were treated thermally before the rheological property analyses and the hyphenated studies. All specimens were dried at 80 °C for 19 h under vacuum, cooled, and kept at around 46 °C for the span of the investigation.

4.3. Characterization Techniques. *4.3.1. Rheological Analyses.* Rheological analyses were conducted using a Physica MCR501 rheometer (Anton Paar Austria) equipped with 25 mm parallel plates. Time-resolved rheology measurements were carried out under an air atmosphere at a strain amplitude of 0.5% (linear region) for 2 h. The selected frequency for the blends were probed at different frequencies of 0.1, 0.3, 1, 3, 6.28, 10, 30, 60, and 100 rad/s to cover the low, intermediate, and high-frequency regions. The time evolution rheological properties of the blends were determined at 230, 240, and 250 °C.

4.3.2. Hyphenated Studies (TGA−FTIR−MS). The effects of the temperature and the time on the thermal degradation and the cross-linking reaction of PA/EVOH and the blend nanocomposites were investigated using thermogravimetric analysis (TGA, PerkinElmer, Pyris 1) coupled with Fourier transform infrared spectroscopy (FTIR, PerkinElmer, Frontier NIR), gas chromatography (GC, PerkinElmer, Clarus 680), and mass spectrometry (MS, PerkinElmer, Clarus SQ 8C). The online measurements (without GC separation) allow the identification of all mass fragments evolved during pyrolysis (TGA in a nitrogen environment) of the blends and the blend nanocomposites. The gas molecules/mass fragments evolved during TGA (isothermal at 230 and 240 °C and temperature ramping) were transferred to the FTIR cell and, finally, to the GCMS via a TG−IR−GCMS interface (TL 9000). The column used to transfer the gas molecules from FTIR to MS (without GC separation) was a SUPELCO analytical SPB-50 fused silica capillary column (30 m long with a diameter of 250 μm). The GC oven temperature was maintained at 280 °C throughout the experiment. The mass/charge ratio analyzed by MS ranged from 35 to 300, and the carrier gas was helium. The isothermal and the ramp methods are presented in Scheme 7a,b, respectively. At the end of the experiment, the furnace was left closed to ensure the environment was not disturbed for FTIR and MS data collection. The sample masses used for this analysis ranged from 21 to 23 mg.

■ ASSOCIATED CONTENT

Supporting Information

The Supporting Information is available free of charge on the ACS Publications website at DOI: 10.1021/acsomega.9b00940.

Rheological degree of conversion β as a function of time for PA/EVOH, PA/EVOH/BET, PA/EVOH/MB, and PA/EVOH/PP-*g*-MA at different temperatures obtained from $G'(t_{\omega=4\ rad/s})$; rate of the rheological degree of conversion $\frac{d\beta}{dt}$ as a function of the degree of conversion β for PA/EVOH, PA/EVOH/BET, PA/EVOH/MB, and

DOI: 10.1021/acsomega.9b00940
ACS Omega 2019, 4, 9569−9582

PA/EVOH/PP-*g*-MA at different temperatures obtained from Figure 1S; rheokinetic parameters obtained from the fittings from equations (2S, 4S) at three temperatures (230, 240, 250 °C) and frequency of 4 rad/s; MS analysis of the gas evolved during the thermal degradation of PA/EVOH blend, PA/EVOH/BET nanocomposite, PA/EVOH/MB nanocomposite, and PA/EVOH/PP-*g*-MA blend at isothermal temperatures of 230, 240, and 250 °C after (a−d) 5 and (a′−d′) 118 min; MS analysis of the gas evolved during thermal degradation of PA/EVOH blend, PA/EVOH/BET nanocomposite, PA/EVOH/MB nanocomposite, and PA/EVOH/PP-*g*-MA blend after 19.6, 23.9, and 27.6 min (PDF)

AUTHOR INFORMATION

Corresponding Authors

*E-mail: Rsalehiyan@csir.co.za (R.S.).
*E-mail: JBandyopadhyay@csir.co.za (J.B.).
*E-mail: rsuprakas@csir.co.za, ssinharay@uj.ac.za (S.S.R.).

ORCID

Reza Salehiyan: 0000-0001-5345-5162
Suprakas Sinha Ray: 0000-0002-0007-2595

Author Contributions

§R.S. and J.B. equally contributed to this work.

Notes

The authors declare no competing financial interest.

ACKNOWLEDGMENTS

The authors would like to acknowledge the Council for Scientific and Industrial Research (HGER74P) and the Department of Science and Technology (HGERA8X) for financial support.

REFERENCES

(1) Cerruti, P.; Laurienzo, P.; Malinconico, M.; Carfagna, C. Thermal oxidative stability and effect of water on gas transport and mechanical properties in PA6-EVOH films. *J. Polym. Sci., Part B: Polym. Phys.* **2007**, *45*, 840−849.

(2) Gorrasi, G.; Incarnato, L.; Vittoria, V.; Acierno, D. Structural characterization of nylon 6/EvOH system through transport properties. *J. Macromol. Sci., Part B: Phys.* **2000**, *39*, 79−92.

(3) Incarnato, L.; Acierno, D.; Russo, P.; Malinconico, M.; Laurienzo, P. Influence of composition on properties of nylon 6/EVOH blends. *J. Polym. Sci., Part B: Polym. Phys.* **1999**, *37*, 2445−2455.

(4) Lagaron, J. M.; Giménez, E.; Saura, J. J. Degradation of high barrier ethylene−vinyl alcohol copolymer under mild thermal-oxidative conditions studied by thermal analysis and infrared spectroscopy. *Polym. Int.* **2001**, *50*, 635−642.

(5) Yeh, J. T.; Yao, W. H.; Du, Q.; Chen, C. C. Blending and barrier properties of blends of modified polyamide and ethylene vinyl alcohol copolymer. *J. Polym. Sci., Part B: Polym. Phys.* **2005**, *43*, 511−521.

(6) Kotal, M.; Bhowmick, A. K. Polymer nanocomposites from modified clays: Recent advances and challenges. *Prog. Polym. Sci.* **2015**, *51*, 127−187.

(7) Salehiyan, R.; Ray, S. S. Influence of nanoclay localization on structure−property relationships of polylactide-based biodegradable blend nanocomposites. *Macromol. Mater. Eng.* **2018**, *303*, No. 1800134.

(8) Salehiyan, R.; Ray, S. S. Processing of Polymer Blends, Emphasizing: Melt Compounding; Influence of Nanoparticles on Blend Morphology and Rheology; Reactive Processing in Ternary Systems; Morphology−Property Relationships; Performance and Application Challenges; and Opportunities and Future Trends. In *Processing of Polymer-Based Nanocomposites*; Springer, 2018; pp 167−197.

(9) Salehiyan, R.; Ray, S. S. Tuning the conductivity of nanocomposites through nanoparticle migration and interface crossing in immiscible polymer blends: A review on fundamental understanding. *Macromol. Mater. Eng.* **2019**, *304*, No. 1800431.

(10) Bandyopadhyay, J.; Ray, S. S.; Salehiyan, R.; Ojijo, V.; Khoza, M.; Wesley-Smith, J. Effect of the mode of nanoclay inclusion on morphology development and rheological properties of nylon6/ethyl−vinyl-alcohol blend composites. *Polymer* **2017**, *126*, 96−108.

(11) Matisová-Rychlá, L.; Lanska, B.; Rychlý, J. Application of chemiluminescence to polymer degradation studies. Thermal oxidation of polyamide 6. *Angew. Makromol. Chem.* **1994**, *216*, 169−186.

(12) Dong, W.; Gijsman, P. Influence of temperature on the thermo-oxidative degradation of polyamide 6 films. *Polym. Degrad. Stab.* **2010**, *95*, 1054−1062.

(13) Carlsson, D.; Chmela, S.; Wiles, D. The oxidative degradation of ethylene/vinyl alcohol copolymers. *Polym. Degrad. Stab.* **1991**, *31*, 255−267.

(14) Morrison, F. A. *Understanding Rheology, Topics in Chemical Engineering*; Oxford University Press: New York, 2001.

(15) Salehiyan, R.; Malwela, T.; Ray, S. S. Thermo-oxidative degradation study of melt-processed polyethylene and its blend with polyamide using time-resolved rheometry. *Polym. Degrad. Stab.* **2017**, *139*, 130−137.

(16) Filippone, G.; Carroccio, S.; Curcuruto, G.; Passaglia, E.; Gambarotti, C.; Dintcheva, N. T. Time-resolved rheology as a tool to monitor the progress of polymer degradation in the melt state−Part II: Thermal and thermo-oxidative degradation of polyamide 11/organo-clay nanocomposites. *Polymer* **2015**, *73*, 102−110.

(17) Filippone, G.; Carroccio, S.; Mendichi, R.; Gioiella, L.; Dintcheva, N. T.; Gambarotti, C. Time-resolved rheology as a tool to monitor the progress of polymer degradation in the melt state−Part I: Thermal and thermo-oxidative degradation of polyamide 11. *Polymer* **2015**, *72*, 134−141.

(18) Kruse, M.; Wagner, M. H. Time-resolved rheometry of poly (ethylene terephthalate) during thermal and thermo-oxidative degradation. *Rheol. Acta* **2016**, *55*, 789−800.

(19) Mours, M.; Winter, H. Time-resolved rheometry. *Rheol. Acta* **1994**, *33*, 385−397.

(20) Hagen, R.; Salmén, L.; Stenberg, B. Effects of the type of crosslink on viscoelastic properties of natural rubber. *J. Polym. Sci., Part B: Polym. Phys.* **1996**, *34*, 1997−2006.

(21) Malkin, A. Y.; Kulichikhin, S. G. *Rheokinetics: Rheological Transformations in Synthesis and Reactions of Oligomers and Polymers*; John Wiley & Sons, 2008.

(22) Hu, J.; Shan, J.; Zhao, J.; Tong, Z. Isothermal curing kinetics of a flame retardant epoxy resin containing DOPO investigated by DSC and rheology. *Thermochim. Acta* **2016**, *632*, 56−63.

(23) Nnyigide, O. S.; Hyun, K. Effects of anionic and cationic surfactants on the rheological properties and kinetics of bovine serum albumin hydrogel. *Rheol. Acta* **2018**, *57*, 563−573.

(24) Guo, Z.; Shen, Y.; Fang, Z. Compatibilization of polyamide 6/poly(2, 6-dimethyl-1, 4-phenylene oxide) blends by poly(styrene-co-maleic anhydride). *J. Polym. Eng.* **2014**, *34*, 193−199.

(25) Chen, J. C. Improved Processing Stability of Ethylene Vinyl Alcohol Polymer Compositions. US Patent, US5260371A, 1993.

(26) Zhang, J.; Wang, A. Study on superabsorbent composites. IX: Synthesis, characterization and swelling behaviors of polyacrylamide/clay composites based on various clays. *React. Funct. Polym.* **2007**, *67*, 737−745.

(27) Maji, P. K.; Das, N. K.; Bhowmick, A. K. Preparation and properties of polyurethane nanocomposites of novel architecture as advanced barrier materials. *Polymer* **2010**, *51*, 1100−1110.

(28) Kuruma, M.; Rao, B. N.; Jana, T. Functionalized polybutadiene diol based hydrophobic, water dispersible polyurethane nano-

DOI: 10.1021/acsomega.9b00940
ACS Omega 2019, 4, 9569−9582

composites: Role of organoclay structure. *Polymer* **2016**, *99*, 404−416.
(29) Bondon, A.; Lamnawar, K.; Maazouz, A. Experimental investigation of a new type of interfacial instability in a reactive coextrusion process. *Polym. Eng. Sci.* **2015**, *55*, 2542−2552.
(30) Hsiao, S.-H.; Liou, G.-S.; Kung, Y.-C.; Lee, Y.-J. Synthesis and characterization of electrochromic poly (amide−imide) s based on the diimide-diacid from 4, 4′-diamino-4″-methoxytriphenylamine and trimellitic anhydride. *Eur. Polym. J.* **2010**, *46*, 1355−1366.
(31) Artzi, N.; Khatua, B.; Tchoudakov, R.; Narkis, M.; Berner, A.; Siegmann, A.; Lagaron, J. Physical and chemical interactions in melt mixed Nylon-6/EVOH blends. *J. Macromol. Sci., Part B: Phys.* **2004**, *43*, 605−624.
(32) Achhammer, B. G.; Reinhart, F. W.; Kline, G. M. Mechanism of the degradation of polyamides. *J. Appl. Chem.* **1951**, *1*, 301−320.

DOI: 10.1021/acsomega.9b00940
ACS Omega 2019, 4, 9569−9582